PCCP

Accepted Manuscript

ROYAL SOCIETY OF CHEMISTRY

www.rsc.org/pccp

CREATED USING THE RSC LaTeX PCCP ARTICLE TEMPLATE – SEE www.rsc.org/electronicfiles FOR DETAILS

ARTICLE TYPE www. rsc.org/xxxxxx | XXXXXXXX

Integrated computational materials discovery of Silver doped Tin Sulfide as a thermoelectric material.†

Chandan Bera,[a] Stephane Jacob,[b] Ingo Opahle[a], N. S. Harsha Gunda[a], Radoslaw Chmielowski[b], Gilles Dennler[b] and Georg K. H. Madsen*[a]

Received Xth XXXXXXXXXX 20XX, Accepted Xth XXXXXXXXX 20XX

First published on the web Xth XXXXXXXXXX 200X

DOI: 10.1039/b000000x

Accelerating the discovery of new materials is crucial for realizing the vision of need-driven materials development. In the present study we employ an integrated computational and experimental approach to search for new thermoelectric materials. High-throughput first principles calculations of thermoelectric transport coefficients are used to screen sulfide compounds conforming to the boundary conditions of abundant and innocuous components. A further computational screening step of substitutional defects is introduced, whereby SnS doped with monovalent cations is identified as having favorable transport properties. By silver doping of SnS under S-rich conditions an electric conductivity more than an order of magnitude above previous reports is realized. The obtained thermoelectric power-factor at room temperature is comparable to the state of the art for thermoelectric materials based on earth abundant, non-toxic elements. The high-throughput screening of extrinsic defects solves a long standing bottle-neck in searching for new thermoelectric materials. We show how the intrinsic carrier concentration in the low-temperature phase of SnSe is two orders of magnitude higher than in SnS. We furthermore find that the carrier concentration in SnSe can still be further optimized by silver doping.

1 Introduction

The decreasing fossil fuel supplies and increasing greenhouse emissions mean that the need for new materials for energy applications is urgent. High-throughput computational materials science shows great promise for accelerating the discovery of new materials [1] and a number of predictions have been realized experimentally. [2] However, present studies tend to focus on optimizing one materials property whereas an optimal material will often be a compromise of several properties determined by boundary conditions imposed by the envisioned application. It is thus a central vision, e.g. of the materials genome initiative, that a more rapid materials deployment should be achievable by covering several processes in the materials continuum when searching for new materials. To realize this vision there is still a strong need to integrate high-throughput computational materials science more with experimental efforts.

In converting waste heat to electric power, thermoelectric materials (TEs) can improve the energy efficiency of combustion engines or harvest the energy from nuclear decay or sunlight. While present research on TEs to a large degree is focused on improving their conversion efficiency [3,4], the state of the art in efficiency is already highly competitive for energy harvesting at low power levels. [5] However, to make a large impact TEs should also be based on low-cost, abundant and innocuous elements, which is a serious issue with several present TEs. [7] This makes TEs a prime example of materials which could benefit from a more broad search for new materials. If the energy is otherwise simply lost to the environment, even materials with a performance well below the state of the art will be interesting provided their cost is moderate. [6]

With this in mind we have set up an intermediate throughput procedure, where computational screening is integrated with the synthesis and actual testing of the TEs. First the thermoelectric coefficients are calculated as a function of doping for a number of binary sulfides. These are screened together with parameters describing the availability of the cations, thereby identifying SnS as potential candidate. While the interesting band structure of SnS [8] has been pointed out and several studies have computationally screened thermoelectric properties, [9–11] it has been a problem of such studies that they lead to the suggestion of a large number of *potential* materials without a clear priority. The key bottle-neck has been that the predicted thermoelectric properties can be at doping levels that are not experimentally achievable. [12,13] It is known that intrinsic SnS has a carrier concentration that is too low for

† Electronic Supplementary Information (ESI) available: Calculated transport properties. Details of defect thermochemistry calculations. Defect thermodynamics of SnSe. Details of carrier concentration calculations. See DOI: 10.1039/b000000x/

[a] *Department of Atomistic Modelling and Simulation, ICAMS, Ruhr-Universität Bochum, Germany. Fax: +49 234 32 14977; Tel: +49 234 32 29313; E-mail: georg.madsen@rub.de*

[b] *IMRA Europe S.A.S., 06904 Sophia Antipolis, France.*

thermoelectric purposes.[14–16] We therefore introduce a second screening step where a range of potential extrinsic dopants are tested computationally. Thereby the monovalent cations are identified as favorable. Using spark-plasma sintering silver doped SnS is realized and a conductivity that is more than an order of magnitude higher than previous reports is realized. The obtained thermoelectric power-factor at room temperature is comparable to the state of the art for thermoelectric materials based on earth abundant, non-toxic elements.

2 Results and discussion

2.1 Screening the thermoelectric properties

We have computationally screened the thermoelectric potential of a range of binary sulfides according to several criteria, as shown in Fig. 1. First of all, we use indicators based on the calculated band structures of the materials[9] namely σ/τ and $PF/\tau = S^2\sigma/\tau$, where σ is the electrical conductivity, S the Seebeck coefficient and τ the electronic relaxation time. We thus rely on a constant relaxation time approximation also for comparing different structures. This means that the calculated PF/τ should be viewed more as descriptor whose sorting order is expected to be highly correlated to the actual experimentally achievable power factors, rather than a prediction of the latter.

Instead of searching for the maximal performance as a function of doping we compare the thermoelectric properties at a doping level of $2 \cdot 10^{19}$ cm^{-3}. Based on previous findings this seems to be a realistic value for sulfides.[17,18] Using a fixed doping level means that σ/τ can be viewed as an inverse effective mass indicator and a high effective mass can potentially have a detrimental effect on thermoelectric properties.[19] Furthermore, we use three economic indicators, namely the abundance of the cation in the earth crust[20] and the Herfindahl-Hirschman Indexes (HHIs).[7] The HHIs quantify whether the production (HHI_P) or reserves (HHI_R) are monopolized. Almost all present TEs would fail at least one of these tests. Tellurium is as rare as Gold and Platinum and even Bismuth and Selenium have a very low natural abundance. Antimony is available in the mega-ton range, but, like the rare-earths, has a a high HHI_P and is almost entirely produced by one country, thereby increasing the risk of supply manipulation.

While the importance of cost considerations will depend on the actual application, a practical tool for visualizing the different demands are the radar plots, Fig. 1. Finding a new TE with favorable thermoelectric properties at realistic doping levels under the conditions of abundance and low HHIs obviously constitutes a significant challenge. One compound GaS scores high on the *PF* indicators but also has a high HHI_P due to Ga, Fig. 1. Two compounds, HfS_2 and SnS_2 (both in the layered CdI_2 structure) show good *PF* indicators but have high effective masses which could be a problem. One possibility is SnS, which scores high as a *p*-type material. This is interesting as the material is known to be intrinsically *p*-type[15,16] and has been reported to have a low thermal conductivity of 1.7 W/Km.[21]

2.2 Doping SnS

The main problem of SnS as a thermoelectric material is that the resistivity of undoped samples is far too high for thermoelectric applications, with the lowest value measured being $\rho = 10$ Ωcm.[22] This high intrinsic resistivity is due to a very low intrinsic carrier concentration ($\sim 10^{16}$ cm^{-3})[14–16], indicating that extrinsic defects must be introduced to optimize the carrier concentration. The carrier concentration in a heavily doped semi-conductor is controlled by the formation of charged defects and there exists a well-established methodology for their study.[23,24] The stability of a defected structure in equilibrium with its surroundings is written as

$$E_d(D,q,\mu) = E_f(D,q) + \sum_\alpha n_\alpha \mu_\alpha + q_e \mu_e \qquad (1)$$

where $E_f(D,q) = E(D,q) - E_{bulk} + \sum_\alpha n_\alpha E_\alpha$ is the defect formation energy with respect the standard state of the defect. $E(D,q)$ is the total energy of a supercell containing the defect D and an extra charge q and E_{bulk} is the energy of the host material, i.e. perfect supercell with no defect. n_α is the number of atoms removed from the defected cell and transferred to the reservoir and E_α is the total energy of their standard state. In the supercell approach $E(D,q)$ must contain a correction for the interaction of the image charges.[25,26] We have used a fixed unit cell with a monopole correction as detailed in the supplementary material. q_e is the number of electrons transferred to the reservoir and μ_e their chemical potential with respect to the valence band maximum.

The chemical potentials of the defect atoms, μ_α in Eq. (1), can be controlled by the experimental growth conditions, but are subject to certain bounds. In the case of SnS, to avoid precipitation of S, Sn or SnS_2, these are given by

$$\mu_{Sn} \leq 0 \quad , \quad \mu_S \leq 0 \quad , \quad \mu_{Sn} + 2\mu_S \leq 3\Delta H_f(SnS_2) \qquad (2)$$

where the formation energy is normalized to the number of atoms. Furthermore, to maintain a stable host

$$\mu_{Sn} + \mu_S = 2\Delta H_f(SnS) \qquad (3)$$

Fig. 2 shows the energy of the most stable intrinsic defects, the vacancies labeled V_{Sn} and V_S, as a function of μ_e in the Sn- and S-rich limits. Fig. 2 illustrates how, in the Sn-rich limit, the chemical potential will be pinned to the center of the band gap by the co-existence of the acceptor-like V_{Sn}^{2-} and donor-like V_S^{2+} vacancies. In the excess sulfur side,

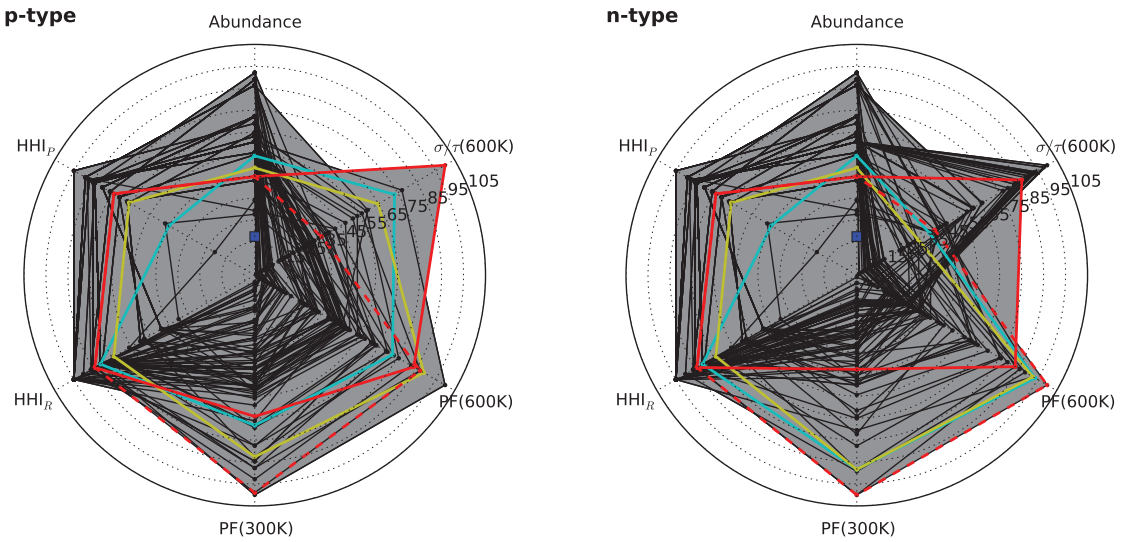

Fig. 1 Radar plots of the abundance, supply risk (HHIproduction and HHIreserve) and calculated thermoelectric power factor $PF = S^2\sigma/\tau$ and σ/τ for a range of binary sulfides. Each ring corresponds to one calculated semi-conducting phase. Four compounds are marked with colored paths, namely red: SnS and SnS_2 (dashed line), cyan: GaS and yellow: HfS_2. Transport properties calculated at a carrier concentration of $2 \cdot 10^{-19}$ cm^{-3} are shown. The crustal abundance is on a logarithmic scale so that Osmium is zero and Oxygen 100. The HHIs are given as 100-HHI/100. The power factor PF/τ and the conductivity σ/τ are scaled so that the maximum value within the full dataset is 100. The blue point marks the abundance of Te. Details of the calculated thermoelectric properties can be found in the supplementary material.

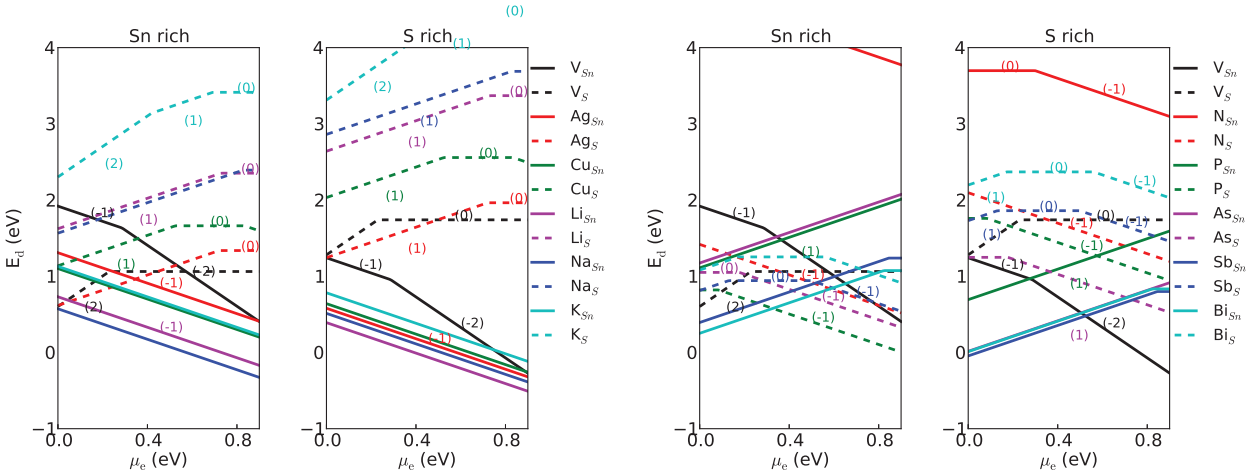

Fig. 2 Defect formation energies for Sn- rich and S -rich limits in SnS as a function of the electron chemical potential. The slopes of the lines correspond to the charge of the defect as marked for the vacancy. The full lines and dashed lines correspond to defects on the Sn and S positions respectively.

SnS would exhibit *p*-type conductivity, due to mainly the acceptor-like V_{Sn}^{2-} vacancy. However, the carrier concentration (see also Fig. 6) due to intrinsic defects would be very low, in agreement with experimentally reported values.[14–16] Compared to an earlier study of the intrinsic defects in SnS[27], we predict a higher formation energy of V_{Sn} in the sulfur rich limit. The difference corresponds quite well to setting $\mu_S = 3\Delta H_f(SnS_2) - 2\Delta H_f(SnS)$, Eqs. (2) and (3), instead of simply using $\mu_S = 0$, indicating that the earlier study did not include precipitation of SnS_2 for limiting the chemical potentials.

To identify the favorable extrinsic defects for optimizing the carriers in SnS, we introduce a second computational screening step. Due to the intrinsic *p*-type carriers it seems most favorable to optimize the hole carrier concentration. In the formally $Sn^{2+}S^{2-}$ valent compound it is natural to look at the monovalent valent cations (Li, Na, K, Cu, Ag, Au, Tl, Hg) as substitutions on the Sn position and the tri-valent anions (N, P, As, Sb and Bi) as substitutions on the S position. Apart from the poisonous Tl and Hg and the highly expensive Au, we have calculated the formation energies of all these defects, Fig. 2. We have furthermore calculated the entire fourth column and potential triple valent transition metals as potential substitutions but found all these defects to be unfavorable.

Considering first the defects of the monovalent cations, Fig. 2a, it is clear that, if the S-rich condition is maintained during growth, Ag, Cu, Li and Na should increase the hole concentration considerably. The S-rich limit not only destabilizes the unfavorable V_{Sn}, but also stabilizes especially the Ag_{Sn} defect. The advantage of the sulfur rich limit is somewhat smaller for the Cu_{Sn} defect. This can be understood in terms of the diagrams in Fig. 3. There are no competing phases containing silver in the sulfur rich limit, whereas ternary Cu_2SnS_3 adds an extra limit to the equilibrium growth conditions

$$2\mu_{Cu} + \mu_{Sn} + 3\mu_S \leq 6\Delta H_f(Cu_2SnS_3) \qquad (4)$$

in case of Cu defects, Fig. 3. This illustrates how the formation energies of all competing binary and ternary phases have to be calculated to obtain the relevant chemical potential limits.[28] We have introduced the calculation of $E_d(D,q,\mu)$ in a high-throughput environment, which includes the calculation of the reference energies of all the competing phases as they are almost a side product of the screening of the transport properties. However, as these reference energies become increasingly available in repositories such as AFLOWlib and the Materials Project, the computational effort of a defect study will be limited to the calculation of $E(D,q)$, Eq. (1).

Considering next the tri-valent anions, Fig. 2b, it is clear that the phosphorus defect P_S is the energetically most interesting. This is, however, only in the Sn-rich limit where V_S is also low in energy. The combination of these two defects will again pin μ_e to the center of the band-gap and result in a low carrier concentration. The Sb and Bi defects are found to prefer the Sn site, where they will form positively charged defects, alas adding electrons to the system. In combination with the negatively charged intrinsic V_{Sn} these pin μ_e to the center of the gap and lead to very low carrier concentrations. This observation is in good agreement with the experimental efforts to fabricate *n*-type SnS by doping with Bi[29] and Sb.[30] In both cases an almost complete destruction of electrical conductivity was found.

2.3 Experimental realization of SnS:Ag

While the aim for materials based on abundant and low supply risk elements is clear, it is also a clear advantage if the materials can be produced using a simple and cost-effective process from powder metallurgy such as sintering.[31] It is difficult, if not impossible, to consider such processes far from thermodynamic equilibrium using computational methods. However, by integrating the computational procedure we have arrived at one system with a short-list of dopants which can be screened experimentally. The doped materials were produced by mixing SnS and the dopants by grinding and sintered by spark-plasma sintering (SPS) at 550°C. The sintering temperature is below the melting temperature of both SnS and the $Ag_2S/Cu_2S/Li_2S/Na_2S$ phases. The measurement of the Seebeck coefficient and the electrical resistivity was carried out with a Linseis LSR-3. All measurements were performed at 60°C. For Ag doping four experimental series were designed. In the first series up to 15 at% pure Ag was added. The resistivity of 15 at% Ag sample, $\rho = 45$ mΩcm, was about two orders of magnitude lower than that previously observed for a similar sample.[32] However, the corresponding Seebeck coefficient appeared to be lower than 100 μV/K. Furthermore, Ag impurities were visible in the X-ray diffraction patterns for all samples above 2 at% Ag. We therefore prepared another batch of samples with a lower Ag content, whereby a resistivity of $\rho = 78$ mΩcm was obtained. To ensure S-rich conditions, we prepared a set of samples with added sulfur and a set where Ag_2S was added to SnS. Several of these samples showed low resistivity, underlining the importance of the S-rich limit. For 2 at% Ag and 1 at% S we obtained $\rho = 38$ mΩcm and for 0.5 at% Ag_2S, $\rho = 59$ mΩcm. The lowest resistivity is coupled to a high Seebeck coefficient of 275 μV/K which leads to a competitive $PF = 199$ μW/K^{2}m. The *PF* as a function of σ is shown in Fig. 4 for the measured points and the theoretical prediction. As is generally observed for this methodology, a good agreement is found between theory and experiment.[33] It is seen that a rather low relaxation time is needed to get agreement with experiment, which could indicate that a higher *PF* could be obtained if cleaner or more dense samples would be grown. The thick line in Fig. 4 marks carrier concentrations up

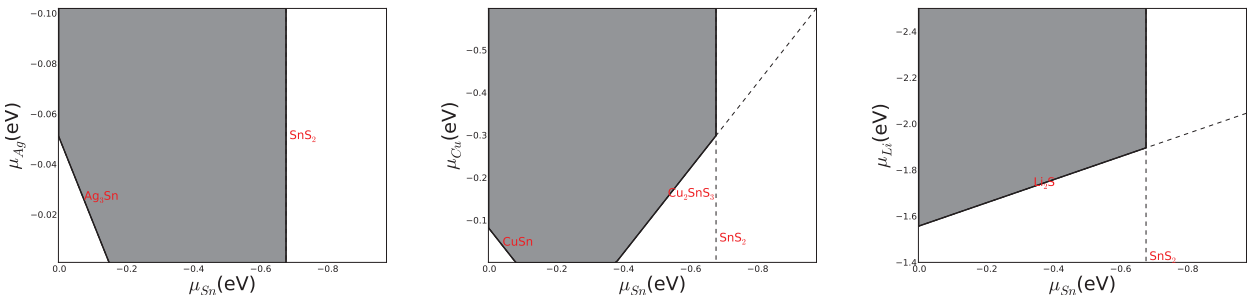

Fig. 3 Calculated chemical potential limits for doping SnS. The shaded areas are the allowed equilibrium growth conditions.

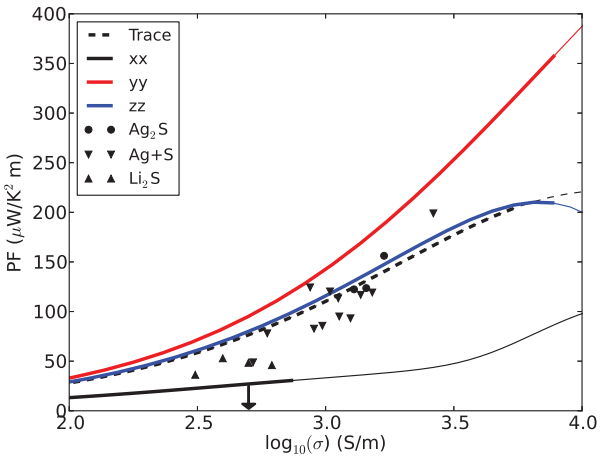

Fig. 4 Power factor vs $\log_{10}(\sigma)$ plot. A $\tau = 3 \cdot 10^{-15}$ s was used. The thicker line marks carrier concentrations up to $p = 2 \cdot 10^{19}$ cm^{-3}. The arrow indicates the highest conductivity previously obtained.[34]. Experimental points are shown for three different doping tests.

to $p = 2 \cdot 10^{19}$ cm^{-3}. This corresponds to the calculated carrier concentration at high annealing temperatures, Fig. 6. Fig. 4 also shows the values calculated along the three directions. It is clear that the conductivity at a given carrier concentration is substantially larger along the *y* and *z* direction, which leads to a substantially higher power factor.

2.4 Carrier concentration in SnSe

During the writing of this manuscript a record *zT* was published for single crystals of SnSe.[35] While we presently have aimed at finding a powder based sulfide material, it is still interesting to compare our results with those for SnSe. Both SnS and SnSe exhibit a phase-transition from the low temperature *Pnma* to a high temperature *Cmcm*-structure. The high *zT* for SnSe was found for the high temperature phase.[35] We have calculated the thermoelectric properties of the *Cmcm*-phase of SnS and also find good thermoelectric properties (see supplementary material). However it is interesting to observe that the phase-transition in SnSe is related to a dramatic increase in carrier concentration, and a resulting increase in electrical conductivity by more than an order of magnitude from below 10 Ω^{-1}cm^{-1} at 500 K to around $\sigma = 100$ Ω^{-1}cm^{-1} at 900 K, following the phase-transition at around 750 K. The low temperature intrinsic carrier concentration in SnSe ($\sim 10^{18}$ cm^{-3}) is still almost two orders of magnitude larger than that found in the iso-structural low-temperature phase of SnS ($\sim 10^{16}$ cm^{-3}).[14–16] Correspondingly the highest measured electrical conductivity at room temperature ($\sigma = 10$ S/cm) is found to be two orders of magnitude higher than the largest found for undoped SnS.[22] The similar ratios between carrier concentration and conductivity indicates that the two compounds have a similar mobility but the intrinsic carrier producing defect, V_{Sn}, is more stable in SnSe. We have confirmed this computationally, Fig. 5. It is seen that the formation energy of the V_{Sn}^{-2} is about 0.5 eV lower in SnSe compared to SnS. Fig. 6 shows the calculated carrier concentration based on the defect formation energies in SnS and SnSe (see supplementary material). As can be seen, the carrier concentration should indeed be about two-orders of magnitude higher in intrinsic *Pnma*-SnSe than in intrinsic *Pnma*-SnS. However, it is interesting to observe that the conductivity of low temperature intrinsic SnSe is still significantly smaller than what we have obtained for the Ag-doped samples ($\sigma = 26$ S/cm the 2 at% Ag, 1 at% S sample). This could mean that the carrier concentration in *Pnma*-SnSe could also be optimized by doping with monovalent cations. This again would mean that the favorable thermoelectric properties are not limited to the high-temperature phase in SnSe. We have confirmed this idea computationally, Fig. 5, and find the Ag_{Sn} defect to have a similar energy as in SnS. Consequently, also in SnSe an increased carrier concentration of the low temperature phase can be expected by Ag doping, Fig. 6, which could increase the

technological interest in this material. This finding is in good agreement with very recent experimental study,[36] which underlines the validity of the present approach.

3 Conclusions

To conclude, we have screened binary sulfides for potential high thermoelectric performance and shown how doping the Sn site in SnS with monovalent cations results in carrier concentrations of thermoelectric relevance. We have experimentally achieved an electric conductivity two orders of magnitude above previous reports and a competitive thermoelectric power-factor.

Our finding of a carrier concentration in SnS is somewhat surprising considering that SnS has received considerable attention for photo-voltaic applications. In this context a $\rho = 7\ \Omega$cm was achieved by adding 15% Ag[32] and $\rho = 200$ mΩcm by adding up to 23% Cu.[34] These values are one to two orders of magnitude larger the results obtained in the present study. One possible explanation of the previously observed low electric conductivity could be that the condition of excess sulfur was not obeyed. This, together with the above mentioned disappointing results when trying to fabricate *n*-type SnS by doping with Bi and Sb[29,30], underlines the value of the computational screening of potential defects when searching for new materials.

While improving the quantitative predictive power of computational defect thermochemistry is still a field of active research,[37] the present work shows that even the standard approach in a high-throughput fashion can give a prioritized

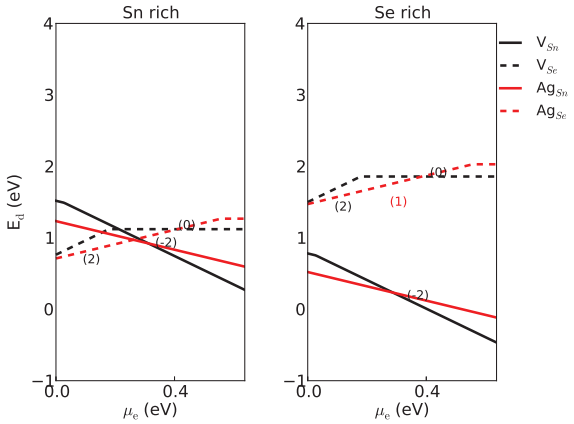

Fig. 5 Defect formation energies for Sn- and Se-rich limits in SnSe in the Pnma structure as a function of the electron chemical potential. The slopes of the lines corresponds to the charge of the defect as marked for the vacancy. The full lines and dashed lines correspond to defects on the Sn and Se positions respectively.

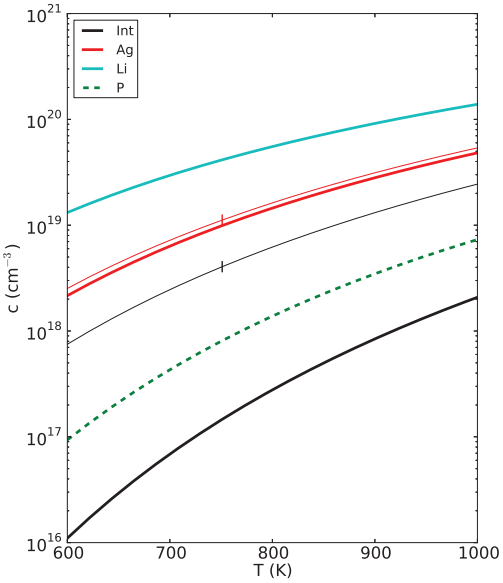

Fig. 6 Carrier concentration due to defects in SnS as a function of fabrication temperature. All lines correspond to the S rich limit except for phosphor doping, which is in the Sn-rich limit. Also shown in thin lines are the calculated carrier concentrations in the low temperature phase of SnSe.

ordering of potential extrinsic dopants. This solves a long-standing problem in the high-throughput search for new thermoelectric materials and demonstrates how high-throughput computational searches can play an important role in widening the range of available thermoelectric materials. This will be especially important as the field matures from a narrow search for improved thermoelectric power factor, to a more broad materials search where several factors play an important role.

References

1 S. Curtarolo, G. L. W. Hart, M. B. Nardelli, N. Mingo, S. Sanvito and O. Levy, *Nature Materials*, 2013, **12**, 191.
2 G. Hautier, A. Jain and S. Ong, *Journal of Materials Science*, 2012, **47**, 7317–7340.
3 J. R. Sootsman, D. Y. Chung and M. G. Kanatzidis, *Angew. Chem. Int. Edit.*, 2009, **48**, 8616–8639.
4 G. J. Snyder and E. S. Toberer, *Nature Materials*, 2008, **7**, 105–114.
5 C. B. Vining, *Nature Materials*, 2009, **8**, 83–85.
6 D. Narducci, *Applied Physics Letters*, 2011, **99**, 102104.
7 M. W. Gaultois, T. D. Sparks, C. K. H. Borg, R. Seshadri, W. D. Bonificio and D. R. Clarke, *Chemistry of Materials*, 2013, **25**, 2911–2920.
8 D. Parker and D. J. Singh, *Journal of Applied Physics*, 2010, **108**, 083712.
9 G. K. H. Madsen, *J. Am. Chem. Soc.*, 2006, **128**, 12140.
10 S. Wang, Z. Wang, W. Setyawan, N. Mingo and S. Curtarolo, *Phys. Rev. X*, 2011, **1**, 021012.
11 I. Opahle, A. Parma, E. J. McEniry, R. Drautz and G. K. H. Madsen, *New Journal of Physics*, 2013, **15**, 105010.
12 E. S. Toberer, A. F. May, C. J. Scanlon and G. J. Snyder, *J. Appl. Phys.*, 2009, **105**, 063701.
13 L. Bjerg, G. K. H. Madsen and B. B. Iversen, *Chemistry of Materials*, 2012, **24**, 2111–2116.
14 W. Albers, C. Haas, H. J. Vink and J. D. Wasscher, *Journal of Applied Physics*, 1961, **32**, 2220.
15 H. Noguchi, A. Setiyadi, H. Tanamura, T. Nagatomo and O. Omoto, *Solar Energy Materials and Solar Cells*, 1994, **35**, 325–331.
16 K. Ramakrishna Reddy, N. Koteswara Reddy and R. Miles, *Solar Energy Materials and Solar Cells*, 2006, **90**, 3041–3046.
17 M.-L. Liu, F.-Q. Huang, L.-D. Chen and I.-W. Chen, *Applied Physics Letters*, 2009, **94**, –.
18 K. Biswas, L.-D. Zhao and M. G. Kanatzidis, *Advanced Energy Materials*, 2012, **2**, 634–638.
19 Y. Pei, A. D. LaLonde, H. Wang and G. J. Snyder, *Energy Environ. Sci.*, 2012, **5**, 7963–7969.
20 Mineral Commodity Summaries 2011; U.S. Department of the Interior, U.S. Geological Survey: Reston, VA, 2011; http://minerals.usgs.gov/minerals/pubs/mcs/2011/mcs2011.pdf.
21 D. Spitzer, *J. Phys. Chem. Solids*, 1970, **31**, 19 – 40.
22 M. M. Nassary and et al, *J. Alloy and Comp.*, 2005, **398**, 21.
23 S. B. Zhang and J. E. Northrup, *Phys. Rev. Lett.*, 1991, **67**, 2339–2342.
24 C. G. Van de Walle, D. B. Laks, G. F. Neumark and S. T. Pantelides, *Phys. Rev. B*, 1993, **47**, 9425–9434.
25 S. Lany and A. Zunger, *Modelling and Simulation in Materials Science and Engineering*, 2009, **17**, 084002.
26 H.-P. Komsa, T. T. Rantala and A. Pasquarello, *Phys. Rev. B*, 2012, **86**, 045112.
27 J. Vidal, S. Lany, M. dAvezac, A. Zunger, A. Zakutayev, J. Francis and J. Tate, *Applied Physics Letters*, 2012, **100**, 032104–032104–4.
28 C. Persson, Y.-J. Zhao, S. Lany and A. Zunger, *Physical Review B*, 2005, **72**, 035211.
29 A. Dussan, F. Mesa and G. Gordillo, *Journal of Materials Science*, 2010, **45**, 2403–2407.
30 P. Sinsermsuksakul, R. Chakraborty, S. B. Kim, S. M. Heald, T. Buonassisi and R. G. Gordon, *Chemistry of Materials*, 2012, **24**, 4556–4562.
31 X. Lu and D. T. Morelli, *Phys. Chem. Chem. Phys.*, 2013, **15**, 5762–5766.
32 M. Devika, N. K. Reddy, K. Ramesh, K. R. Gunasekhar, E. S. R. Gopal and K. T. R. Reddy, *Journal of The Electrochemical Society*, 2006, **153**, G727–G733.
33 L. Bjerg, G. K. H. Madsen and B. B. Iversen, *Chem. Mat.*, 2011, **23**, 3907–3914.
34 S. Zhang and S. Cheng, *Micro & Nano Letters*, 2011, **6**, 559.
35 L.-D. Zhao, S.-H. Lo, Y. Zhang, H. Sun, G. Tan, C. Uher, C. Wolverton, V. P. Dravid and M. G. Kanatzidis, *Nature*, 2014, **508**, 373–377.
36 C.-L. Chen, H. Wang, Y.-Y. Chen, T. Day and G. J. Snyder, *J. Mater. Chem. A*, 2014, –.
37 A. Glensk, B. Grabowski, T. Hickel and J. Neugebauer, *Phys. Rev. X*, 2014, **4**, 011018.